



OPEN ACCESS

EDITED BY

Stefano Masiero,
University of Padua, Italy

REVIEWED BY

Zekeriya Duzgun,
Giresun University, Türkiye
Haotian Li,
Beijing Key Laboratory of Functional
Gastrointestinal Disorders Diagnosis and
Treatment of Traditional Chinese Medicine,
China

*CORRESPONDENCE

Haiyang Yu
✉ gszyxqs@gszy.edu.cn
Jinqiu Wu
✉ 18394025223@163.com

[†]These authors have contributed equally to
this work and share first authorship

RECEIVED 26 October 2025

REVISED 06 January 2026

ACCEPTED 12 January 2026

PUBLISHED 04 February 2026

CITATION

Ma T, Wang D, Xie Q, Li Y, Wang J, Zhang X,
Yuan L, He H, Han X, Liu X, Liu J, Yu H and
Wu J (2026) Identification and validation of
biomarkers of Shenggu Zaizao Wan in the
treatment of steroid-induced osteonecrosis
of the femoral head by integrating network
pharmacology and bulk transcriptomic.
Front. Med. 13:1732825.
doi: 10.3389/fmed.2026.1732825

COPYRIGHT

© 2026 Ma, Wang, Xie, Li, Wang, Zhang, Yuan,
He, Han, Liu, Liu, Yu and Wu. This is an
open-access article distributed under the
terms of the [Creative Commons Attribution
License \(CC BY\)](https://creativecommons.org/licenses/by/4.0/). The use, distribution or
reproduction in other forums is permitted,
provided the original author(s) and the
copyright owner(s) are credited and that the
original publication in this journal is cited, in
accordance with accepted academic
practice. No use, distribution or reproduction
is permitted which does not comply with
these terms.

Identification and validation of biomarkers of Shenggu Zaizao Wan in the treatment of steroid-induced osteonecrosis of the femoral head by integrating network pharmacology and bulk transcriptomic

Tao Ma^{1,2†}, Duoxian Wang^{3†}, Qingsheng Xie¹, Yin Li¹,
Jinpeng Wang¹, Xiaogang Zhang³, Lingwei Yuan², Hairong He²,
Xianfu Han², Xuerui Liu², Jianjun Liu³, Haiyang Yu^{3,4*} and
Jinqiu Wu^{2*}

¹Clinical College of Traditional Chinese Medicine, Gansu University of Chinese Medicine, Lanzhou, China, ²Department of Sports Medicine, Gansu Provincial Hospital of Traditional Chinese Medicine, Lanzhou, China, ³Department of Orthopaedics, Affiliated Hospital of Gansu University of Chinese Medicine, Lanzhou, China, ⁴Department of Orthopaedics, Shenzhen Bao'an Traditional Chinese Medicine Hospital, Shenzhen, China

Background: Steroid-induced osteonecrosis of the femoral head (SONFH) is a debilitating condition. Research has shown that Shenggu Zaizao Wan (SZW) may have therapeutic effects on SONFH. This study aimed to elucidate the mechanisms by which SZW treats SONFH.

Methods: SONFH and control samples were retrieved from a database to identify differentially expressed genes (DEGs). Biomarkers were obtained through the intersection of DEGs and potential targets, machine learning, and expression validation. A nomogram was constructed, followed by gene set enrichment analysis (GSEA) of biomarkers and immune infiltration analysis. Molecular docking was conducted, and the expression of biomarkers was evaluated using real-time quantitative reverse transcription PCR (RT-qPCR).

Results: A total of 69 potential SZW targets and 1,671 DEGs were identified. IKBKB and PRKCA were established as biomarkers for SONFH, and a nomogram was developed. GSEA indicated that IKBKB and PRKCA may influence pathways related to the ribosome. Immune infiltration analysis revealed that CD4⁺ T cells play a role in SONFH. Molecular docking showed a strong affinity between SZW compounds and biomarkers. The expression of biomarkers in clinical samples aligned with the results from bioinformatics analysis.

Conclusion: This study identified IKBKB and PRKCA as potential biomarkers and targets for SZW treatment in SONFH.

KEYWORDS

biomarkers, molecular docking, network pharmacology, Shenggu Zaizao Wan, steroid-induced osteonecrosis of the femoral head

1 Introduction

Steroid-induced osteonecrosis of the femoral head (SONFH) is a skeletal disorder caused by prolonged or excessive glucocorticoid use, characterized by the progressive necrosis of femoral head cells. This can ultimately lead to degenerative arthritis and collapse of the femoral head (1). Each year, approximately 20,000 to 30,000 new cases of SONFH are reported globally (2). The disease progresses rapidly and is associated with a high disability rate, resulting in a substantial economic burden on patients and potentially diminishing their long-term quality of life (3). Due to its destructive nature, early intervention in SONFH is crucial. Current treatment strategies primarily involve conservative therapies such as anticoagulants, vasodilators, statins, bisphosphonates, and physical therapy, along with surgical options like core decompression and total hip replacement (4). Although total hip replacement offers a relatively effective solution for advanced cases, postoperative complications and the need for joint revisions exacerbate the patient's burden, placing additional strain on social healthcare systems (5). Therefore, there is an urgent need for novel therapeutic strategies for SONFH.

In China, traditional Chinese medicine (TCM) has a long history of treating SONFH and plays a significant role in preventing bone cell death and structural damage to the femoral head caused by the condition (6). Shenggu Zaizao Wan (SZW), composed of *Epimedium brevicornu Maxim*, *Davallia trichomanoides Blume*, *Astragalus membranaceus*, *Cinnamomi ramulus*, *Wolfiporia cocos*, *Rhizoma alismatis*, *Salvia miltiorrhiza*, *Panax notoginseng*, *Crataegus pinnatifida Bunge*, and *Psoralea corylifolia L.*, has shown significant clinical efficacy in treating the early and intermediate stages of SONFH. Recent studies suggest that the active components of these herbs are widely used for treating fractures, joint diseases, and various chronic orthopedic conditions, particularly exhibiting notable effects on SONFH (7, 8). Icaritin, the active compound in *Epimedium*, exerts therapeutic effects on femoral head necrosis through anti-inflammatory actions, reduction of vascular damage, prevention of osteocyte apoptosis, promotion of bone marrow mesenchymal stem cell proliferation, reduction of oxidative stress, and inhibition of adipocyte differentiation (9, 10). Additionally, astragaloside IV can alleviate the progression of SONFH by inhibiting endoplasmic reticulum stress (11). Active ingredients such as tanshinone I (TsI) and tanshinone IIA have shown positive effects in antioxidation and antithrombosis (12, 13). Other components also provide vascular protective effects and promote bone repair (14, 15). In recent years, network pharmacology has achieved significant progress in exploring the therapeutic mechanisms of TCM formulas, identifying effective components, and uncovering therapeutic targets. Compared to previous studies on single components, research on the interactions between multiple components and targets offers a more accurate reflection of the *in situ* conditions in clinical practice (16). Despite these advancements, the treatment of SONFH with SZW remains based on TCM theory (17) and lacks modern pharmacological research, leaving its molecular mechanisms unclear. Identifying new targets and molecular mechanisms of SZW and its active components in the treatment of SONFH is of significant importance.

In this study, transcriptomic data related to SONFH were obtained from the Gene Expression Omnibus (GEO) database, and differentially expressed genes (DEGs) were identified. Disease targets associated with SONFH and targets of SZW acting on SONFH were sourced from the Traditional Chinese Medicine Systems Pharmacology Database

and Analysis Platform (TCMSP), Herbal Encyclopedia for Research on Bioactivity and Chemical Constituents (HERB), and GeneCards databases. These targets were then intersected with DEGs to identify candidate genes. Machine learning and expression validation methods were employed to screen potential biomarkers. By integrating the results of Kyoto Encyclopedia of Genes and Genomes (KEGG) enrichment analysis and the protein–protein interaction (PPI) network, the potential molecular mechanisms of these biomarkers in SONFH were elucidated. Finally, molecular docking was used to evaluate the binding affinity of biomarkers to the active ingredients in SZW, verifying the molecular mechanisms of SZW and its active components in the treatment of SONFH. The findings have significant theoretical and practical implications for improving clinical treatments and developing innovative targeted therapeutic agents.

2 Materials and methods

2.1 Data collection

The GEO database¹ provided transcriptome data for SONFH (GSE123568 and GSE74089). The GSE123568 dataset (GPL15207) included 30 SONFH and 10 control blood samples, serving as the training set, while the GSE74089 dataset (GPL13497) contained 4 ONFH and 4 control cartilage tissue samples, used as the validation set.

2.2 Sifting of targets and active components of SZW

SZW consists of 10 components: *Epimedium brevicornu Maxim*, *Davallia trichomanoides Blume*, *Astragalus membranaceus*, *Cinnamomi ramulus*, *Wolfiporia cocos*, *Rhizoma alismatis*, *Salvia miltiorrhiza*, *Panax notoginseng*, *Crataegus pinnatifida Bunge*, and *Psoralea corylifolia L.* Active components and targets for *Epimedium brevicornu Maxim*, *Davallia trichomanoides Blume*, *Astragalus membranaceus*, *Cinnamomi ramulus*, *Wolfiporia cocos*, *Rhizoma alismatis*, *Salvia miltiorrhiza*, and *Panax notoginseng* were obtained from the TCMSP database², using criteria for oral bioavailability (OB) $\geq 30\%$ and drug likeness (DL) ≥ 0.18 . Therapeutic targets for *Crataegus pinnatifida Bunge* and *Psoralea corylifolia L.* were retrieved from the HERB database.³ After integrating all drug targets, standardized SZW targets were acquired via the UniProt database.⁴ A drug–component–target network was constructed using Cytoscape (v 3.10.2) (18) with topological data sourced from TCMSP.

2.3 Screening putative targets of SZW for SONFH intervention

The GeneCards database⁵ was used to obtain SONFH-related targets by merging and deduplicating data with keywords

1 <https://www.ncbi.nlm.nih.gov/geo/>

2 <https://old.tcmsp-e.com/tcmsp.php>

3 <http://herb.ac.cn/>

4 <https://www.uniprot.org/>

5 <https://www.genecards.org/>

“steroid-induced osteonecrosis of the femoral head” and “femur head steroid necrosis.” The final SONFH targets were obtained after merging and deduplication. SZW therapeutic targets for SONFH were identified by intersecting disease-associated targets with compound targets using the VennDiagram package (v 1.7.3) (19). A drug-target-disease network was established using Cytoscape (v 3.10.2) (18).

2.4 Identification of DEGs and candidate genes

The “limma” package (v 3.54.0) (20) was used to identify differentially expressed genes (DEGs) between SONFH and control samples (SONFH vs. control) ($|\log_2\text{FoldChange (FC)}| > 0.5$, $p < 0.05$) from all samples in the GSE123568 dataset. Volcano plots were generated using ggplot2 (v3.3.6) (21) to visualize DEGs, with the ten most significantly up/down-regulated genes annotated. Hierarchical clustering of the top 10 up/down-regulated genes in SONFH vs. controls was visualized using the “ComplexHeatmap” package (v 2.14.0) (22). Candidate genes were identified by intersecting SONFH-related DEGs with SZW therapeutic targets using “VennDiagram” (v 1.7.3).

2.5 Enrichment analysis and construction of PPI network

Candidate genes underwent functional annotation and pathway enrichment analysis using KEGG and GO databases *via* the “clusterProfiler” package (v 4.6.2) (23), with statistical significance set at $p < 0.05$. The top 5 enriched terms in GO and the top 10 terms in KEGG were visualized. A protein–protein interaction (PPI) network was constructed using the Search Tool for the Retrieval of Interacting Genes and Proteins (STRING) database⁶ (confidence ≥ 0.4) to examine the protein-level interactions of candidate genes. The analysis was restricted to *Homo sapiens*, and visual outputs were generated using Cytoscape v3.10.2.

2.6 Machine learning and expression level verification

Biomarker discovery integrated the LASSO regression algorithm, SVM-RFE algorithm, and transcriptomic profiling. LASSO regression (*via* glmnet v4.1-4) (24) and SVM-RFE (svmRadial method using caret v6.0-93) (25) were applied to the GSE123568 cohort. Candidate biomarkers were identified by intersecting genes selected by both algorithms using the “VennDiagram” package (v 1.7.3). Gene expression differences between SONFH and control samples in both the GSE123568 and GSE74089 cohorts were assessed using Wilcoxon testing ($p < 0.05$). Visualization of the results was performed using the “ggplot2” package (v 3.3.6). Genes showing significant differences and consistent expression trends across both datasets were considered biomarkers. For chromosomal localization, RCircos (v 1.2.2) (26) generated genome-wide distribution plots.

6 <https://string-db.org/>

2.7 Construction of the nomogram model

Using the “rms” package (v 6.5-0) (27), a biomarker-driven nomogram was developed to assess diagnostic performance in the GSE123568 dataset. Each biomarker was assigned a score, and the sum of the scores represented the total points. The likelihood of SONFH was predicted based on the total points. The accuracy of the nomogram was evaluated using a calibration curve (*via* the “ResourceSelection” package v 0.3.5)⁷ and the Hosmer-Lemeshow (HL) test ($p > 0.05$, mean absolute error [MAE] < 0.1). Additionally, ROC analysis using pROC v1.18.0 (28) evaluated the diagnostic efficacy of the nomogram (Area Under Curve [AUC] > 0.7).

2.8 GSEA

Gene set enrichment analysis (GSEA) was employed to explore the functional roles of biomarkers in SONFH. The reference gene set used was “c2.kegg.v7.4.symbols,” obtained from the Molecular Signatures Database (MSigDB, <https://www.gsea-msigdb.org/gsea/msigdb/>). Spearman correlation coefficients (using the psych v2.4.3 package) (28) ranked genes based on biomarker association strength. GSEA (*via* clusterProfiler v4.6.2) on GSE123568 identified significant pathways ($P/\text{FDR} < 0.05$), with the top 10 entries prioritized by p -value.

2.9 Analysis of immune cell type abundance

Immune cell infiltration was assessed by ssGSEA for 28 immune cell types (29) in all SONFH and control samples from the GSE123568 dataset. Differential immune cells (DICs) were identified *via* the Wilcoxon test ($p < 0.05$). Correlations between biomarkers and DICs, as well as correlations among DICs, were evaluated using Spearman correlation analysis (*via* the “psych” package v 2.2.9) (30) ($|\text{correlation coefficient (cor)}| > 0.3$, $p < 0.05$). The results were visualized using the “ggplot2” package (v 3.3.6).

2.10 Prediction of factors linked to biomarkers

Transcription factors (TFs) linked to biomarkers were obtained from the NetworkAnalyst database.⁸ miRNAs were retrieved from the miRWalk database⁹ and miRTarBase¹⁰, with miRNAs linked to biomarkers identified by overlapping results from both databases. The lncRNAs associated with these miRNAs were obtained from the miRNet database.¹¹ All data were visualized as previously described.

7 <https://github.com/psolymos/ResourceSelection>

8 <https://www.networkanalyst.ca/>

9 <http://mirwalk.umm.uni-heidelberg.de/>

10 <https://mirtarbase.cuhk.edu.cn/>

11 <https://www.mirnet.ca/>

2.11 Molecular docking

Molecular docking simulations were conducted to assess the binding affinities between prioritized bioactive compounds from SZW and candidate biomarkers. 3D structural coordinates of target biomarkers were retrieved from the RCSB PDB repository¹², while the three-dimensional conformations of bioactive compounds were sourced from PubChem.¹³ Docking simulations were performed using the CB-DOCK platform¹⁴, which automatically executed the entire process, including protein preparation (removal of water molecules and addition of hydrogen atoms), active pocket prediction, grid generation, conformational searching, and scoring. Binding interactions between the bioactive ligands and target biomarkers were analyzed, with a total score threshold of <-5.0 (31).

2.12 RT-qPCR analysis

Biomarker expression was evaluated in blood samples using RT-qPCR. Five SONFH and five control blood samples were collected at the Gansu University of Traditional Chinese Medicine Affiliated Hospital. Informed consent was obtained from all participants, and ethical approval was granted by the Ethics Committee of Gansu University of Traditional Chinese Medicine Affiliated Hospital in May 2023 (protocol code “202,345”). Total RNA was extracted from the paired samples using TRIzol reagent (Vazyme, Nanjing, China), and RNA concentrations were measured by Yi Sheng, Wuhan, China. Complementary DNA (cDNA) was synthesized from mRNA templates through reverse transcription. The cDNA was then diluted with ddH₂O and subjected to RT-qPCR using the following program: pre-denaturation at 95 °C for 1 min, followed by 40 cycles of denaturation at 95 °C for 20 s, annealing at 55 °C for 20 s, and extension at 72 °C for 30 s. The expression levels of biomarkers in SONFH versus control samples were calculated using the $2^{-\Delta\Delta Ct}$ method, and expression differences were assessed using Student's *t*-test ($p < 0.05$). All data processing and visualization were performed using GraphPad Prism software (version 8.0) (32). Detailed primer information and machine testing conditions are provided in Supplementary Table 1.

2.13 Statistical analysis

All statistical analyses and data visualizations were performed using R software (v4.2.2). Specifically, differential expression analysis was conducted using the “limma” package (v 3.54.0); feature selection via LASSO regression was performed using the “glmnet” package (v4.1-4), while support vector machine-recursive feature elimination (SVM-RFE) was conducted with the “caret” package (v6.0-93); functional and pathway enrichment analyses were carried out using the “clusterProfiler” package (v 4.6.2); intersections were visualized with the “VennDiagram” package (v 1.7.3); a nomogram model based on key biomarkers was constructed using the “rms” package (v 6.5-0);

and Spearman correlation analysis was performed using the “psych” package (v 2.2.9). In addition, drug-component-target networks and PPI networks were built and visualized using Cytoscape software (v 3.10.2). For comparisons between groups, Student's *t*-test or Wilcoxon rank-sum test was applied according to the data distribution, with a *p*-value < 0.05 considered statistically significant.

3 Results

3.1 Identification of the potential targets of SZW in the treatment of SONFH

In the TCMSP database, 283 targets and 124 active ingredients were obtained from 8 drugs after deduplication (Supplementary Tables 1, 2). The HERB database provided 13 target proteins. After consolidating and standardizing data from both databases, 125 high-confidence therapeutic targets for SZW were identified (Supplementary Table 3). The network constructed based on the TCMSP database results revealed relationships between 8 drugs, 104 active ingredients (e.g., hederagenin), and 115 targets (e.g., ACACA). In this network, red, purple, and pink represented the 8 drugs, 115 targets, and 104 active ingredients, respectively (Figure 1A). Subsequently, 1,914 disease-related targets were sourced from the GeneCards database (Supplementary Table 4). After intersecting these disease-related targets with compound targets, 69 potential targets were identified as implicated in SZW treatment for SONFH (Figure 1B). The relationships among the drugs, disease, and target genes are shown in Figure 1C, where orange, purple, and pink represent drugs, targets, and diseases, respectively.

3.2 Screening and preliminary analysis of candidate genes

The GSE123568 dataset revealed 1,671 DEGs ($|\log_2FC| > 0.5$, $p < 0.05$), comprising 1,245 up-regulated and 426 down-regulated genes in SONFH samples (Figures 2A,B). Intersection with SZW therapeutic targets identified 11 core candidate genes (Figure 2C). Gene Ontology (GO) analysis highlighted 499 biological processes (BPs), 5 cellular components (CCs), and 56 molecular functions (MFs) significantly enriched ($p < 0.05$) (Figure 2D; Supplementary Table 5). For example, candidate genes were enriched in biological processes related to cytokine-mediated signaling, cellular components such as the CD40 receptor complex, and molecular functions like protein serine/threonine kinase activity. In KEGG analysis, candidate genes were notably enriched in the C-type lectin receptor signaling pathway ($p < 0.05$) (Figure 2E; Supplementary Table 6). The PPI network indicated that the 11 genes were interconnected, with NFE2L2, NFKBIA, and IKBKB showing interactions with multiple genes (Figure 2F).

3.3 Identification of biomarkers

Feature selection through least absolute shrinkage and selection operator (LASSO) ($\log(\lambda_{\min}) = -3.8704$) identified 6 key

¹² <https://www.rcsb.org/>

¹³ <https://pubchem.ncbi.nlm.nih.gov/>

¹⁴ <https://cadd.labshare.cn/cb-dock/php/blinddock.php>

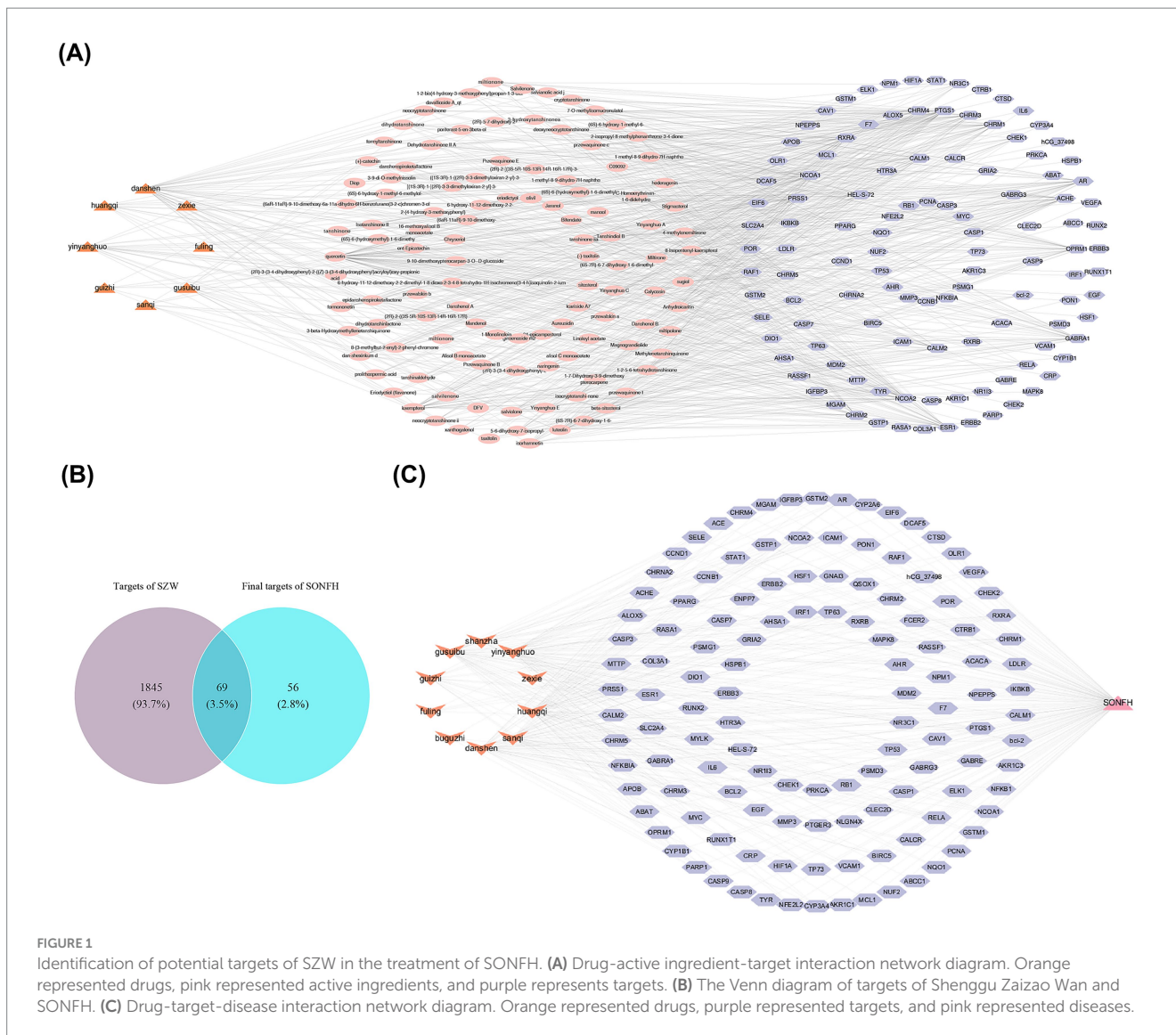


FIGURE 1 Identification of potential targets of SZW in the treatment of SONFH. (A) Drug-active ingredient-target interaction network diagram. Orange represented drugs, pink represented active ingredients, and purple represents targets. (B) The Venn diagram of targets of Shenggu Zaizao Wan and SONFH. (C) Drug-target-disease interaction network diagram. Orange represented drugs, purple represented targets, and pink represented diseases.

genes (Figures 3A,B), complemented by SVM-RFE revealing 8 biomarkers (Figure 3C). A total of 5 candidate biomarkers (NFE2L2, RAF1, IKKB, CASP1, and PRKCA) were selected from the intersection of the two algorithms (Figure 3D). Notably, IKKB and PRKCA showed significant expression differences between SONFH and control samples ($p < 0.05$), with both genes being upregulated in SONFH across two independent datasets (Figures 3E,F). Therefore, IKKB and PRKCA were designated as biomarkers. Chromosomal location analysis revealed that IKKB is located on chromosome 8, while PRKCA is located on chromosome 17 (Figure 3G).

3.4 Construction of a SONFH nomogram

Based on the biomarkers IKKB and PRKCA, a diagnostic nomogram model was constructed to assess SONFH risk (Figure 4A). The calibration curve demonstrated good fit ($p = 0.573$) and low error (MAE = 0.046) (Figure 4B). ROC analysis using the GSE123568 dataset, which was employed to build the model,

showed that the model exhibited strong discriminative ability (AUC = 0.877) (Figure 4C). However, the performance evaluation of this model is based solely on internal data at this stage, and its diagnostic efficacy and clinical applicability require further validation.

3.5 Enrichment pathways of biomarkers

GSEA revealed that IKKB and PRKCA were significantly enriched in 62 and 53 pathways, respectively (Supplementary Table 7, false discovery rate [FDR] < 0.05, $p < 0.05$). Specifically, IKKB was enriched in oxidative phosphorylation (Figure 5A), while PRKCA was enriched in RNA degradation and ubiquitin-mediated proteolysis (Figure 5B). Additionally, both IKKB and PRKCA were enriched in pathways related to the ribosome, spliceosome, and neuroactive ligand receptor interactions. These results suggest that IKKB and PRKCA may play a significant role in the progression of SONFH through these enriched pathways.

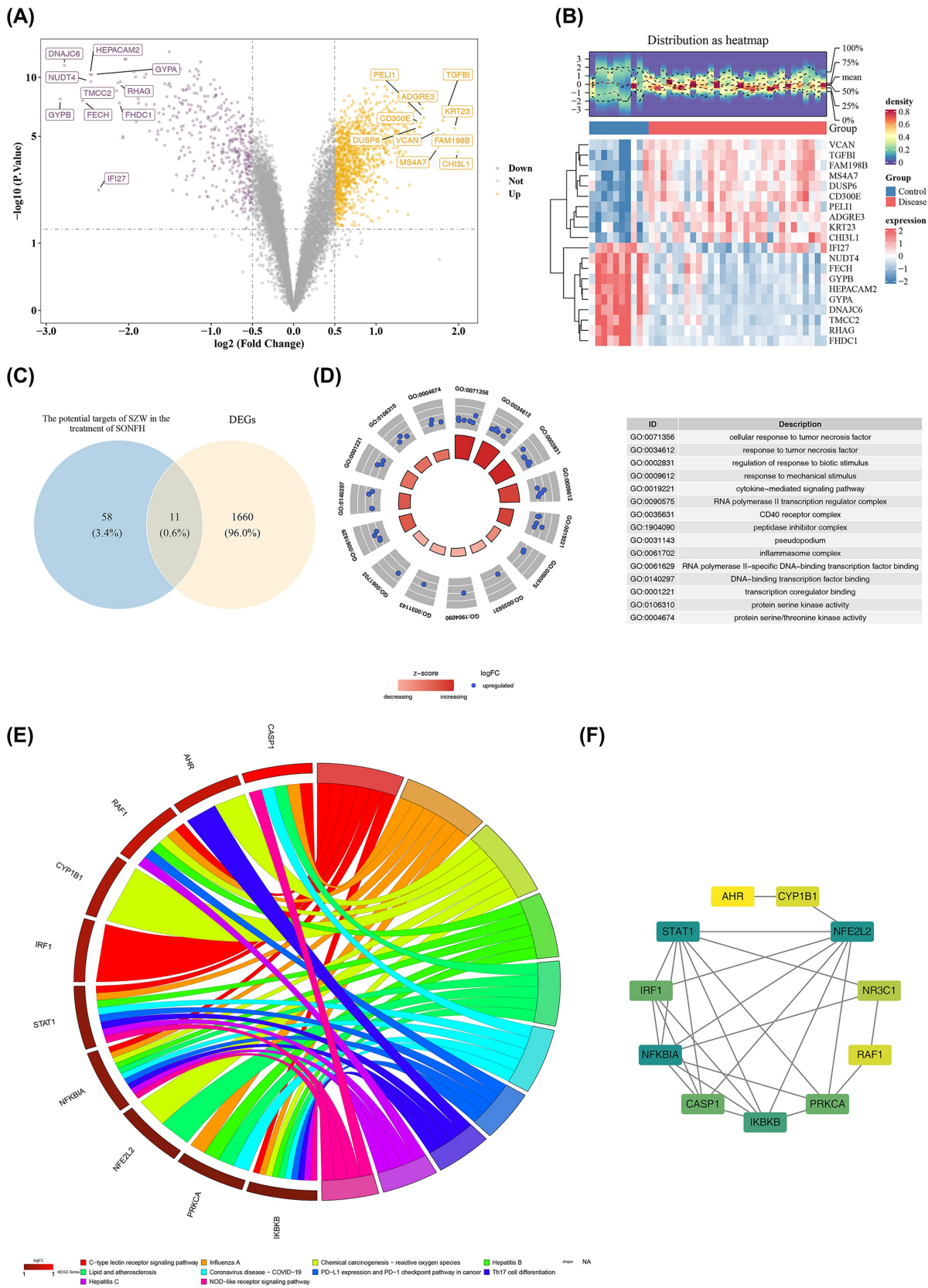


FIGURE 2 Screening and preliminary analysis of candidate genes. **(A)** Volcanic map of differential gene expression between SONFH group and control group. Yellow: Up-regulated gene; Purple: Down-regulated gene. The names of the top 10 genes up and down regulated gene. **(B)** Differential gene

(Continued)

FIGURE 2 (Continued)

expression heatmap between SONFH group and control group. The color represented the expression level of the gene, with higher expression levels indicating a redder color and lower expression levels indicating a bluer color. Red: Disease group; Blue: Control group. (C) Potential targets of Shenggu Zaizao Wan in the treatment of SONFH and the Venn diagram of DEGs. (D) Gene GO enrichment circle diagram of candidate genes. Each GO entry had a corresponding circle, and the color inside the circle represented the logFC value of the entry, where blue represented upregulation expression. (E) KEGG pathway enrichment string plot of candidate genes. Each line represented a different molecular mechanism. (F) PPI network diagram. The degree of the protein encoded by genes corresponded to colors ranging from yellow to green from small to large.

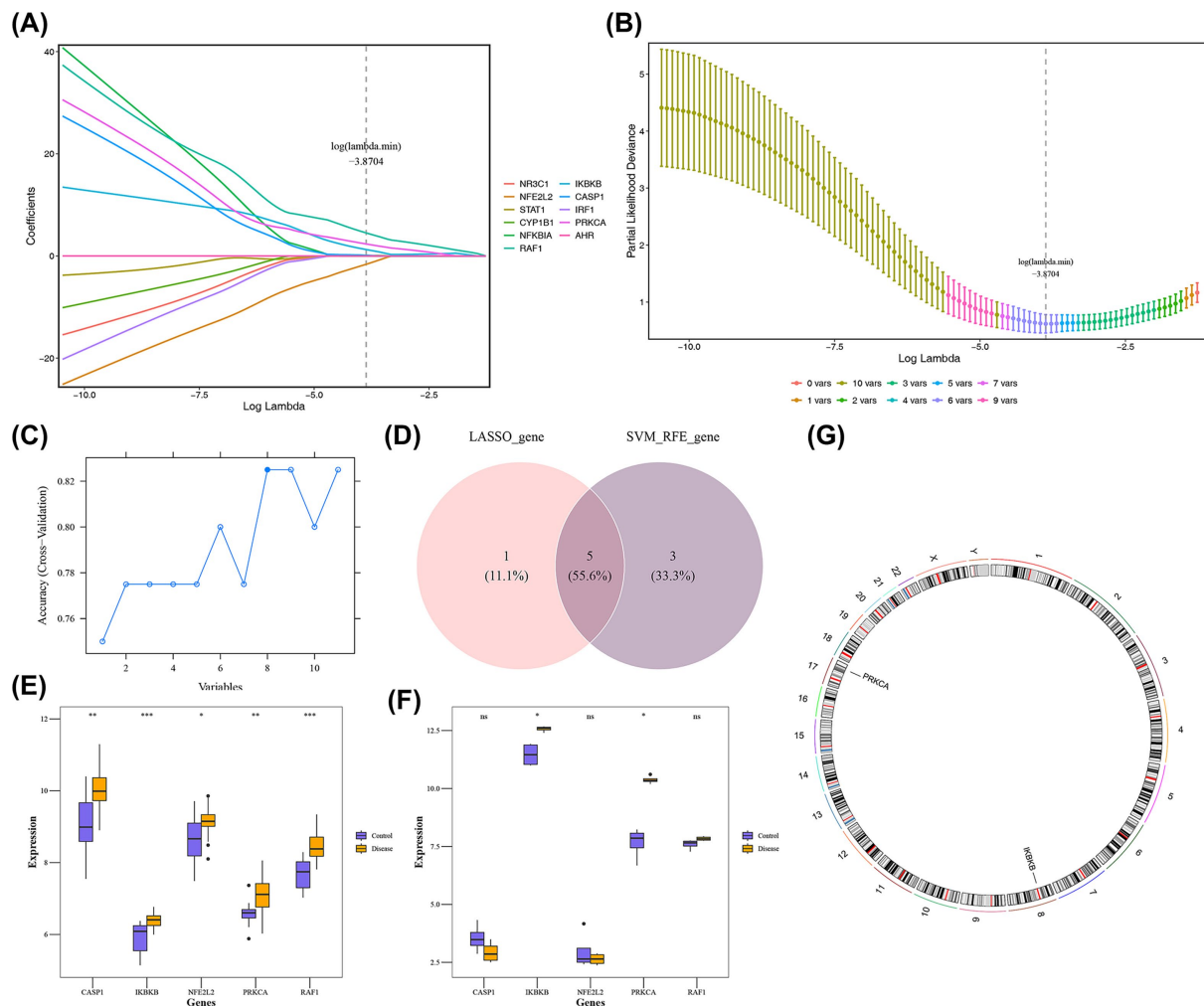


FIGURE 3

Identification of biomarkers (A,B) Lasso analysis of candidate genes. When reaching the optimal lambda, remove variables with coefficients equal to 0. (C) Construction of SVM-RFE model. The blue solid dots represented the potential feature genes screened out when the model reached the highest accuracy after the first 8 features. (D) Venn diagram of characteristic genes of LASSO and SVM-RFE. (E,F) Box plot of expression levels of potential key genes in the training set and validation set. Purple: Control group; Yellow: Disease group. ns: $p \geq 0.05$; *: $p < 0.05$; **: $p < 0.01$; ***: $p < 0.001$. (G) Chromosome localization analysis of key genes. The outer circle of the image corresponded to the position of the chromosome, while the inner circle represented the position information of key genes on the chromosome.

3.6 Immune cells linked to biomarkers in SONFH

To evaluate the systemic immune status of patients with SONFH, the relative abundance of 28 immune cell subsets was quantified using single-sample GSEA (ssGSEA) based on whole-blood transcriptome data from the GSE123568 dataset. As illustrated in Figure 6A, distinct patterns were observed in the abundance profiles of various immune cell subtypes between the SONFH and control groups. Wilcoxon analysis

revealed significant differences in the abundance of 22 immune cell subsets (e.g., activated CD8⁺ T cells) between SONFH and control groups ($p < 0.05$) (Figure 6B). Correlation analysis indicated a significant positive association between activated CD8⁺ T cells and central memory CD4⁺ T cells ($cor = 0.79, p < 0.001$), as well as between macrophages and neutrophils ($cor = 0.78, p < 0.001$) (Figure 6C; Supplementary Table 8). Further analysis showed robust positive correlations between IKKKB ($cor = 0.72, p < 0.01$) and PRKCA ($cor = 0.75, p < 0.01$) with central memory CD4⁺ T cells (Figure 6D; Supplementary Table 9). These results

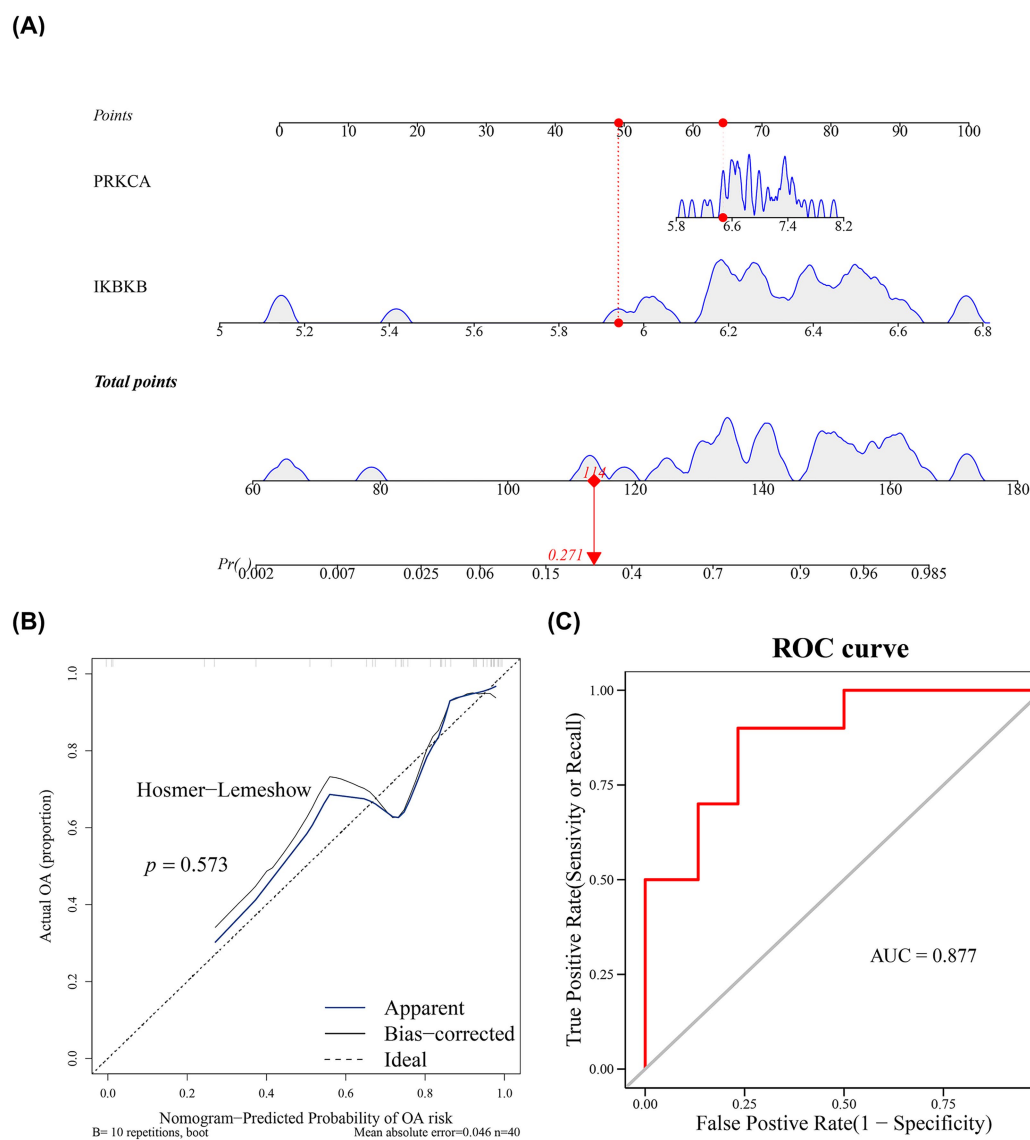


FIGURE 4

Construction of nomogram. **(A)** Nomogram of key genes. The horizontal axis of two genes represented the expression level of the genes. **(B)** Calibration curve of key genes. The black dashed line represented a perfect prediction. The blue solid line represented the entire queue, and the black solid line is used for deviation correction through bootstrap (1,000 repetitions), indicating the observed column chart performance. **(C)** ROC curve analysis chart. The closer the AUC value was to 1, the stronger the predictive performance.

suggest that these differentially infiltrated cells (DICs), particularly central memory CD4⁺ T cells, may have a significant impact on SONFH.

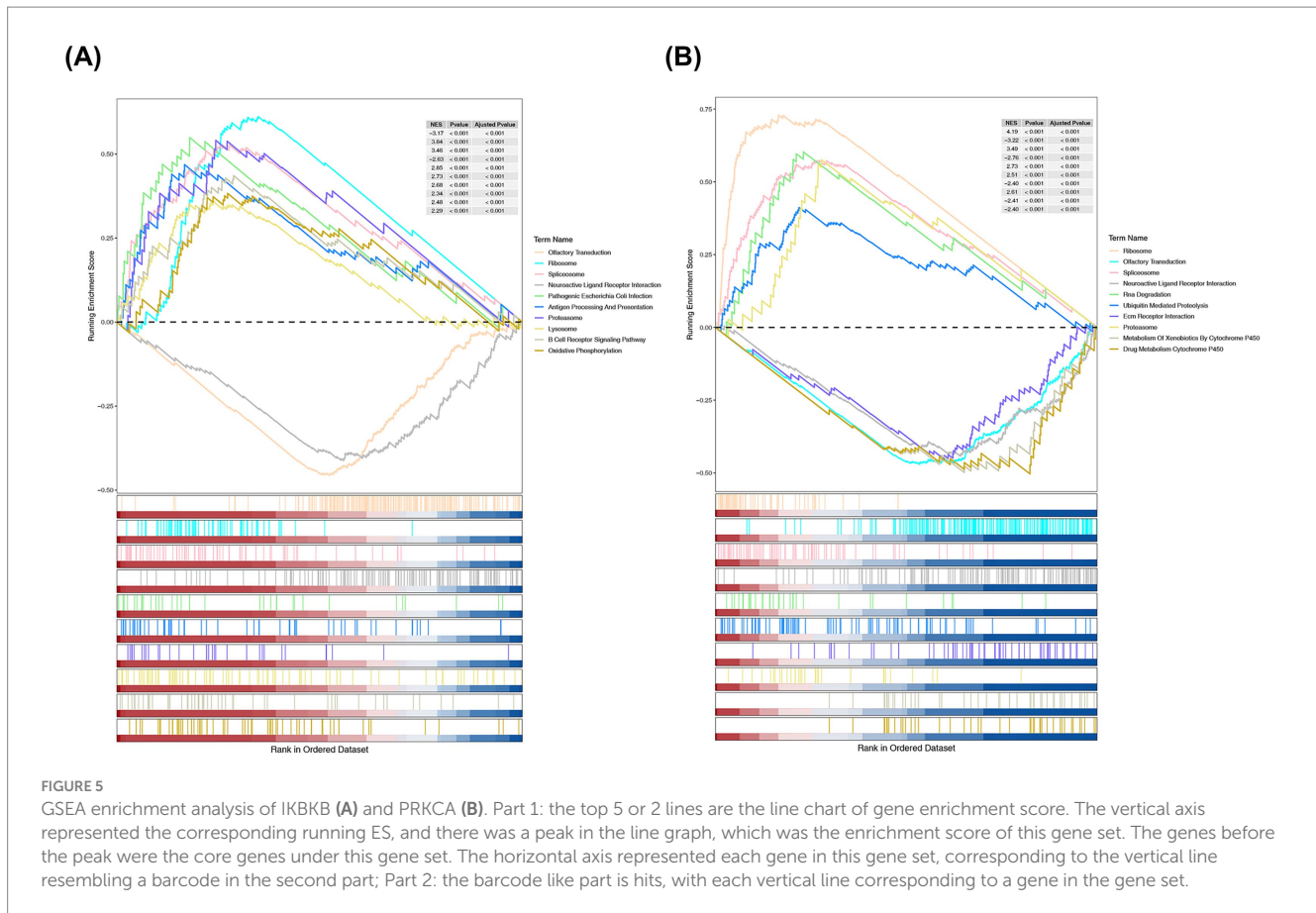
3.7 Construction of network

A total of 14 TFs, including SPI1 and SCRT2, were linked to IKBKB, while 30 TFs, such as ADNP, were associated with PRKCA (Figure 7A). Among these, two TFs, MLLT1 and BCL11B, were predicted to be linked to FBP1 and RHOG. Furthermore, three miRNAs, including hsa-miR-196a-5P, were found to be associated with IKBKB (Figures 7B,D). A total of 22 miRNAs, such as hsa-miR-24-3p and hsa-miR-17-3p, were linked to PRKCA (Figures 7C,E). Additionally, nine miRNAs were found to have corresponding lncRNAs, with 260 lncRNAs (including MDS2, H19, and SNHG11) linked to these miRNAs. In total, the biomarkers-miRNAs-lncRNAs network incorporated 9 miRNAs, 260 lncRNAs, and

the two biomarkers (Figure 7). These factors associated with the biomarkers may play important roles in the progression of SONFH.

3.8 Molecular docking between active components of SZW with biomarkers

A total of 14 active ingredients of SZW were selected for molecular docking with IKBKB and PRKCA, and the total scores are presented in Table 1. Trametenolic acid (total score = -7.7) (Figure 8A) and tanshinone IIA (total score = -7.6) (Figure 8B) exhibited stronger binding affinity with PRKCA compared to other active ingredients, while (-)-taxifolin (total score = -7.1) (Figure 8C) and luteolin (total score = -6.9) (Figure 8D) demonstrated greater binding affinity with IKBKB. Additional findings are provided in Supplementary Figure 1. These results suggest that these active ingredients may more effectively



modulate the biological activity of SONFH-related targets in the respective drugs.

3.9 Real-time quantitative reverse transcription PCR (RT-qPCR) experiments of biomarkers

RT-qPCR experiments with clinical samples revealed significant differences in the expression of IKBKB and PRKCA between SONFH and control samples ($p < 0.05$) (Figures 9A,B). The expression patterns of these genes were consistent with the results of our bioinformatics analysis, further validating the reliability of our current findings.

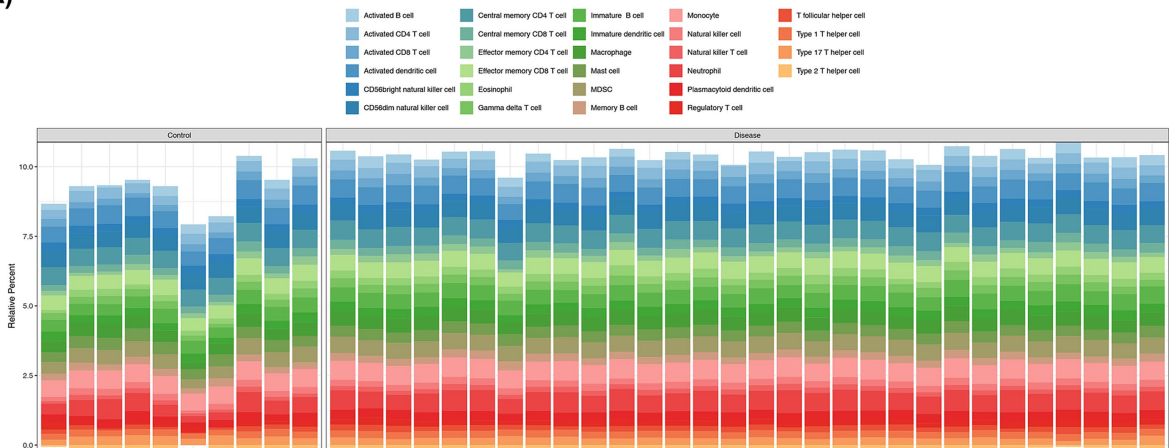
4 Discussion

SONFH is a destructive osteoarticular disease caused by long-term and excessive glucocorticoid use, resulting in femoral head collapse, hip pain, and functional impairment (33). The treatment of SONFH presents numerous challenges, highlighting the need for new therapeutic strategies. Using network pharmacology, this study initially identified 283 targets and 124 active components, with Inhibitor of Nuclear Factor Kappa B Kinase Subunit Beta (IKKBK) and Protein Kinase C Alpha (PRKCA) identified as key biomarkers for the therapeutic effects of SZW on SONFH. Additionally, the potential molecular mechanisms of these biomarkers in SONFH were analyzed through KEGG enrichment analysis and PPI network

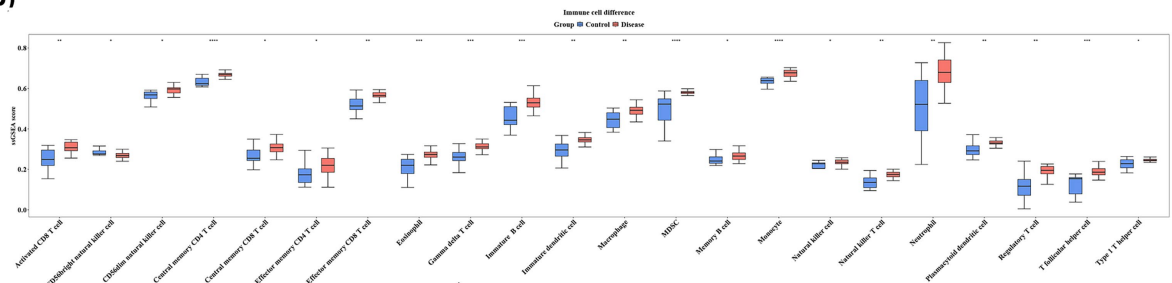
construction. GSEA results suggested that IKBKB and PRKCA may be involved in SONFH progression through pathways related to ribosomes, spliceosomes, and other mechanisms. Immune infiltration analysis revealed that activated CD8⁺ T cells, central memory CD4⁺ T cells, and other immune cell types may significantly impact SONFH. Molecular docking results further demonstrated that certain active ingredients of SZW exhibit strong binding affinities with these biomarkers. Additionally, RT-qPCR analysis showed significant differences in the expression levels of IKBKB and PRKCA between SONFH and control samples. The core innovation of this study lies in the identification of the association between the clinical formula SZW and two key signaling molecules (IKKBK and PRKCA), whose roles in SONFH have not been fully elucidated. This study provides modern scientific evidence for the traditional Chinese herbal compound SZW, laying a theoretical foundation for further mechanistic exploration and optimization of its clinical application.

IKKBK encodes the IKK β protein, which functions as the central kinase in the NF- κ B classical signaling pathway. Along with IKK α and NEMO (IKK γ), IKK β forms the IKK kinase complex responsible for phosphorylating and degrading the I κ -B α protein. This degradation releases RelA/p50 dimers, allowing them to translocate to the nucleus and regulate the expression of target genes (34). Biallelic mutations in IKKBK that result in loss of function cause severe combined immunodeficiency, characterized by reduced T cell populations, developmental abnormalities, and impaired immune responses (35). Additionally, IKKBK plays a pivotal role in B cell maturation, immune responses, cell survival, and the production of antigen-specific antibodies (36). It is also involved in antigen

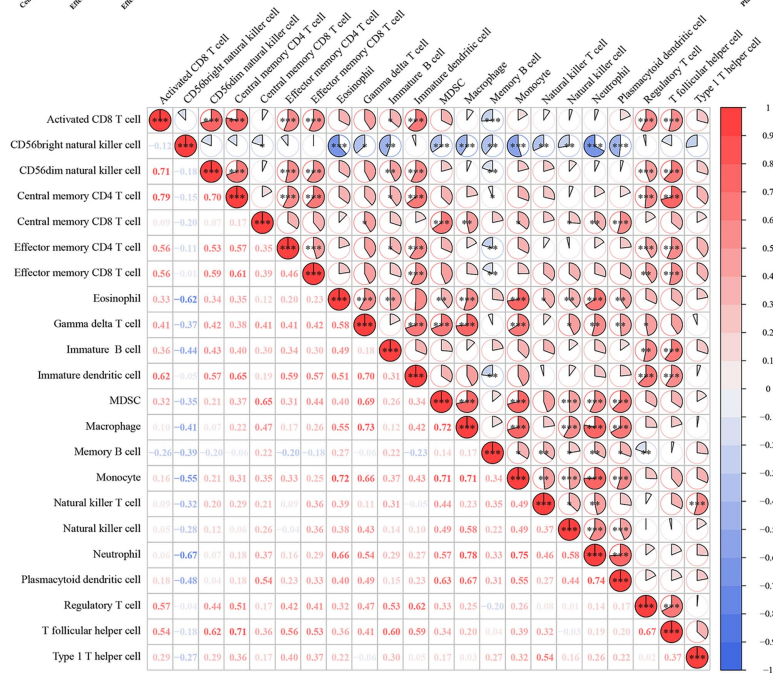
(A)



(B)



(C)



(D)

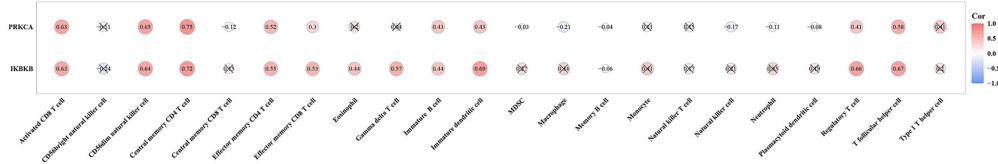


FIGURE 6 Immune cells linked to biomarkers in SONFH. (A) The proportion of immune cells in each sample. (B) Twenty-two immune infiltrating cells based on enrichment score boxplots between disease group and control group. Red: Disease group; Blue: Control group. *: $p < 0.05$; **: $p < 0.01$; ***: $p < 0.001$;

(Continued)

FIGURE 6 (Continued)
 ****: $p < 0.0001$. (C) Correlation heatmap between 22 different immune cells. The redder the color, the stronger the positive correlation, and the bluer the color, the greater the negative correlation coefficient. *: $p < 0.05$; **: $p < 0.01$; ***: $p < 0.001$. (D) Correlation heatmap between 22 differential immune cells and 2 biomarkers. The redder the color, the stronger the positive correlation, and the bluer the color, the greater the negative correlation coefficient.

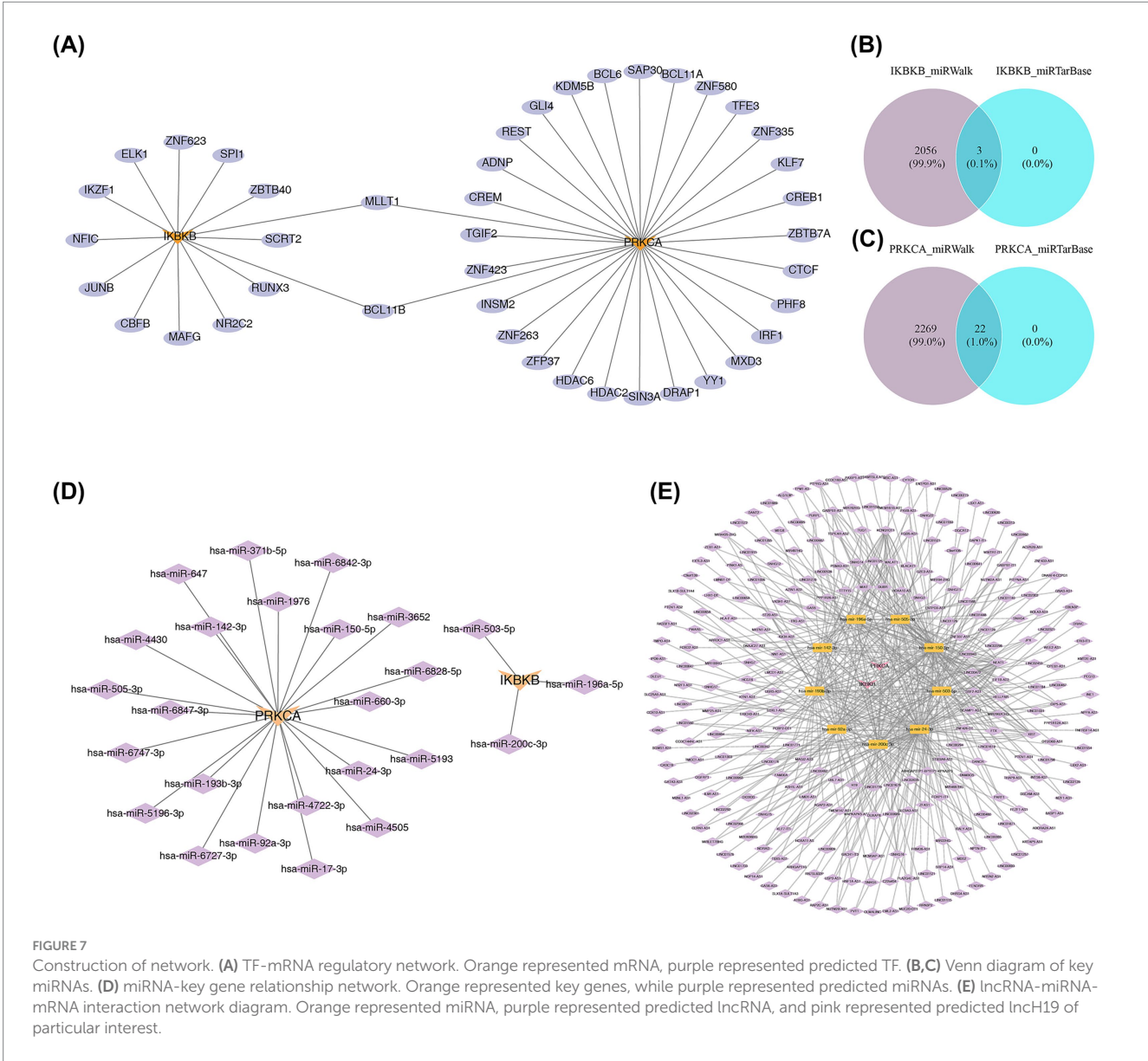


FIGURE 7

Construction of network. (A) TF-mRNA regulatory network. Orange represented mRNA, purple represented predicted TF. (B,C) Venn diagram of key miRNAs. (D) miRNA-key gene relationship network. Orange represented key genes, while purple represented predicted miRNAs. (E) lncRNA-miRNA-mRNA interaction network diagram. Orange represented miRNA, purple represented predicted lncRNA, and pink represented predicted lncH19 of particular interest.

presentation and immune functions in dendritic cells and macrophages, emphasizing its widespread influence on the immune system (37, 38). Previous research has shown that NF-κB signaling mediated by NF-κB-inducing kinase (NIK) is vital for osteoclast differentiation (39). A study further indicated that circIKBKB is upregulated in breast cancer bone metastasis tissues, and its overexpression enhances osteoclastogenesis, promoting the formation of a pre-metastatic niche (40). Moreover, studies on SONFH have demonstrated a significant correlation between IKBKB expression and immune cell function (41). The present study found a notable increase in IKBKB transcription levels in patients with

SONFH, and clinical sample validation further corroborated these findings, suggesting that IKBKB plays a role in SONFH progression. Molecular docking analysis in this study revealed that the active components taxifolin and luteolin in SZW have a high binding affinity for the IKBKB protein, suggesting that SZW may regulate IKBKB. Existing literature reports that both taxifolin and luteolin inhibit the activation of the NF-κB signaling pathway (42, 43). Based on the observed upregulation of IKBKB in SONFH and its role in the NF-κB pathway, SZW may target IKBKB through components like taxifolin and luteolin, modulating its kinase activity and preventing excessive NF-κB activation. This could be a potential mechanism

TABLE 1 Molecular docking score.

Active ingredients of SZW	Drugs	Gene	Total score
24-epicampesterol	Epimedium brevicornu Maxim	IKBKB	-6.6
		PRKCA	-7.1
Pinoresinol	Davallia trichomanoides Blume	IKBKB	-6.3
		PRKCA	-5.9
Mairin	Astragalus membranaceus	IKBKB	-6.4
		PRKCA	-7
(-)-taxifolin	Cinnamomi ramulus	IKBKB	-7.1
		PRKCA	-7
Trametenolic acid	Wolfiporia cocos	IKBKB	-6.8
		PRKCA	-7.7
Sitosterol	Rhizoma alismatis	IKBKB	-6.4
		PRKCA	-7
Poriferasterol	Salvia miltiorrhiza	IKBKB	-6.6
		PRKCA	-7.2
DFV	Panax notoginseng	IKBKB	-6.3
		PRKCA	-6.7
Bakuchalcone	Psoralea corylifolia	IKBKB	-6.8
		PRKCA	-7.2
Quercetin	Epimedium brevicornu Maxim, Astragalus membranaceus, Panax notoginseng	IKBKB	-6.7
		PRKCA	-6.9
Kaempferol	Epimedium brevicornu Maxim, Davallia trichomanoides Blume, Astragalus membranaceus	IKBKB	-6.3
		PRKCA	-7
Luteolin	Epimedium brevicornu Maxim, Davallia trichomanoides Blume, Salvia miltiorrhiza	IKBKB	-6.9
		PRKCA	-6.8
Tanshinone IIA	Salvia miltiorrhiza	IKBKB	-6.5
		PRKCA	-7.6

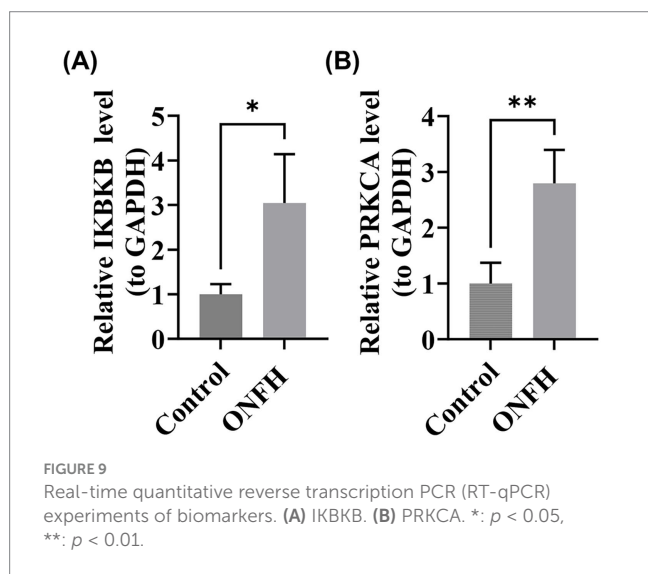
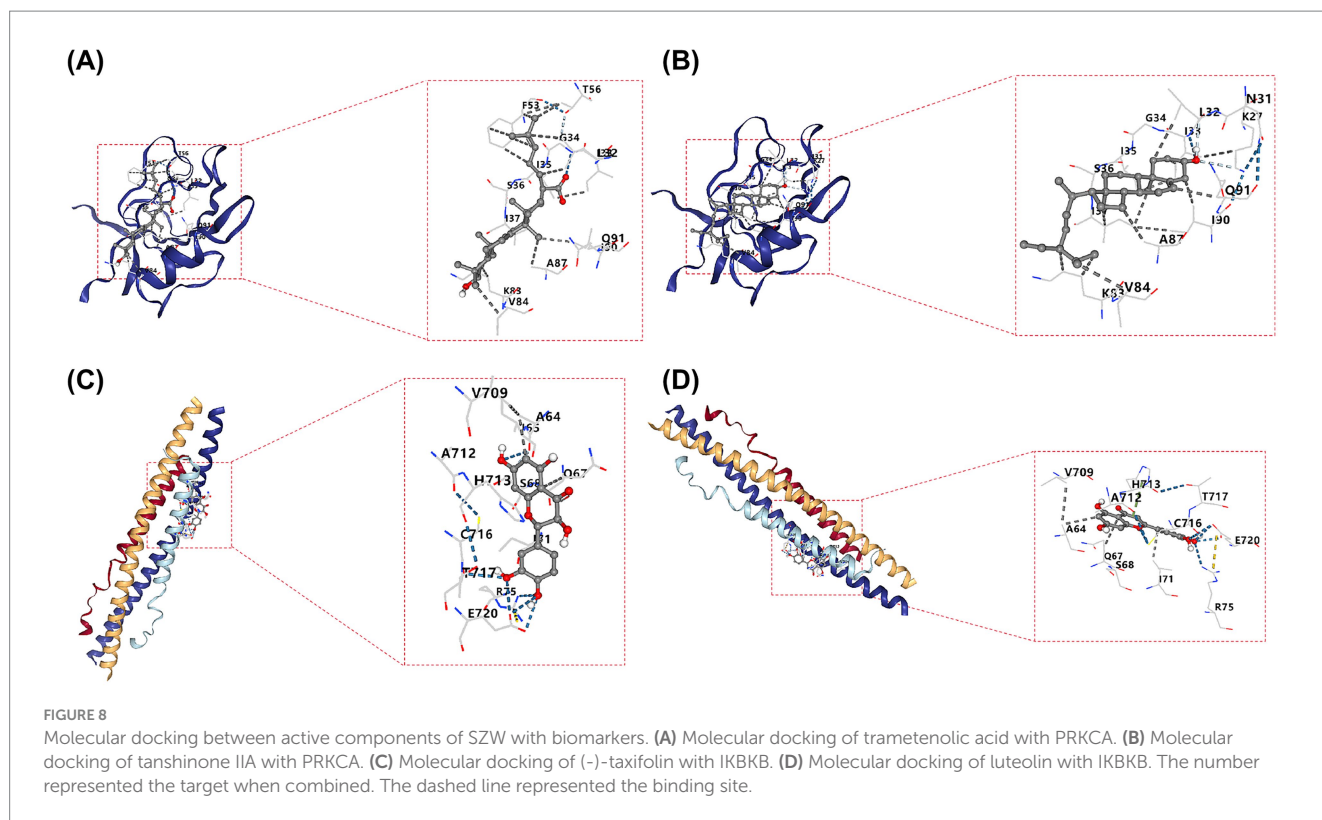
through which SZW alleviates inflammation in SONFH, regulates immune cell function, and suppresses abnormal bone resorption. However, this hypothesis requires experimental validation in SONFH models to directly confirm whether SZW and its specific components exert therapeutic effects *via* IKBKB.

PRKCA is a member of the serine/threonine-specific protein kinase C family, involved in mediating cell growth and inflammatory responses (44). Overexpression of PRKCA inhibits the secretion of lipopolysaccharide (LPS)-induced inflammatory factors, including IL-1 β , TNF- α , and IL-6, thereby alleviating sepsis-induced acute lung injury in mice. PRKCA and its encoded protein kinase (PKC α) primarily regulate cellular proliferation, differentiation, and anti-apoptotic signaling, making them pivotal in tumor formation and chemotherapy resistance (45). PKC α inhibits osteoblast differentiation while promoting osteoblast proliferation (46),

highlighting its role in regulating the cellular signaling involved in osteoblast differentiation and proliferation. However, the detailed molecular regulatory mechanisms of PRKCA remain unclear, requiring further investigation, particularly in the context of osteonecrosis of the femoral head. This study identified a significant upregulation of PRKCA expression in both SONFH clinical samples and public transcriptomic data (GSE123568), suggesting its potential involvement in the pathological progression of SONFH. Similarly, molecular docking results revealed high binding affinity between tanshinone IIA, an active component of SZW, and PRKCA. Previous studies have confirmed that tanshinone IIA inhibits osteoclast differentiation and bone resorption (47). Based on these findings, SZW may modulate PRKCA through components such as tanshinone IIA, influencing its downstream signaling pathways. This mechanism could help regulate the balance between osteogenesis and osteoclastogenesis, potentially offering bone-protective effects in SONFH. Future research is needed to further investigate the specific role of PRKCA in SONFH and determine whether it serves as a direct target for SZW's therapeutic effects, providing additional evidence for SZW in treating SONFH.

According to the GSEA results, IKBKB is significantly enriched in the oxidative phosphorylation pathway, while PRKCA is enriched in the RNA degradation and ubiquitin-mediated proteolysis pathways. Both IKBKB and PRKCA may be closely associated with SONFH through multiple pathways, including the ribosome, spliceosome, proteasome, olfactory transduction, and neuroactive ligand-receptor interactions. The spliceosome, an RNA-protein complex responsible for mRNA splicing, enables alternative splicing, allowing a single gene to produce several proteins through various exon arrangements (48). Circular RNAs (circRNAs), byproducts of precursor mRNAs, act as sponges to regulate miRNA activities, facilitate gene translation *via* alternative splicing, and interact with RNA-binding proteins (RBPs) (49). Additionally, circRNAs play a role in the physiological and pathological processes of various orthopedic diseases, including osteosarcoma, osteoporosis, and osteoarthritis (50–52). Notably, our findings suggest that spliceosomes may also play a pivotal role in SONFH.

Analysis of peripheral blood immune cell composition revealed significant alterations in the proportions and activity of multiple immune cell subsets in patients with SONFH, including macrophages, neutrophils, activated CD8⁺ T cells, and central memory CD4⁺ T cells. Correlation analysis indicated that activated CD8⁺ T cells exhibited the strongest association with biomarkers, suggesting they may exert a considerable influence on the biomarkers associated with SONFH. Research has demonstrated the presence of neutrophil extracellular traps in the microvascular system surrounding the femoral head in patients with osteonecrosis, suggesting a role for neutrophils in the pathogenesis of SONFH (35). Additionally, studies have shown that macrophages and monocytes serve as sources of osteoclasts, with osteoclast-mediated bone resorption being a critical mechanism in femoral head collapse (53, 54). Previous reports have linked macrophages to bisphosphonate-related osteonecrosis of the jaw and steroid-induced osteonecrosis (55), indicating a close relationship between macrophages and SONFH. A retrospective clinical controlled study revealed that the total lymphocyte count, CD3T cells, Ts cells (CD3CD8), and B-1 cells (CD5CD19) in the peripheral blood of patients with femoral head necrosis were significantly elevated,



suggesting an association between the occurrence and progression of femoral head necrosis and immune system imbalances (56). However, this study is based on blood sample analysis, directly reflecting changes in circulating immunity. The involvement of these systemic immune characteristics in the local osteonecrotic process of SONFH requires future validation using lesioned tissue samples or experimental models that more closely replicate the pathological process.

To construct TF-mRNA pairs, two TFs, MLLT1 and BCL11B, were identified as being associated with the key genes IKBKB and PRKCA. Three miRNAs associated with IKBKB, including hsa-miR-503-5P and hsa-miR-196a-5P, were identified, along with twenty-two

miRNAs related to PRKCA, such as hsa-miR-24-3P. Furthermore, 260 lncRNAs regulating IKBKB and PRKCA expression were identified, with nine of these lncRNAs serving as effective predictors. In recent years, an increasing number of miRNAs have been implicated in osteonecrosis, with mechanisms such as coagulation disorders, abnormal apoptosis, and lipid metabolism dysregulation identified as contributors (57–59). Additionally, lncRNAs can competitively bind to miRNAs through the “sponge effect,” regulating the proliferation and function of osteoblasts (60). Therefore, these TFs, miRNAs, and lncRNAs may play a significant role in SONFH progression by modulating the expression of biomarkers and influencing disease progression.

This study has several limitations. First, the clinical sample size used for RT-qPCR validation was relatively small, which, although providing preliminary evidence for differential expression, may impact statistical power and limit the generalizability of the findings. Second, the validation dataset (GSE74089) used for trend observation differed from the primary training set in terms of tissue origin and disease scope, potentially introducing contextual interference in the interpretation of gene expression consistency. Additionally, due to research timeline constraints and challenges in sample collection, this study did not establish an intervention group for SZW. As a result, while upregulation of IKBKB and PRKCA was observed in patients with SONFH, it cannot be conclusively confirmed that these factors are the direct therapeutic targets of SZW. Consequently, the related conclusions remain speculative and association-based. Furthermore, although the nomogram diagnostic model demonstrated good discriminatory performance in internal data, the sample size in the training cohort was limited, and independent validation in large, homogeneous clinical cohorts was lacking. The absence of systematic comparisons with existing diagnostic methods further complicates its

potential clinical applicability. Therefore, further verification is needed to assess its clinical translation.

To address these limitations, future research will focus on several directions: constructing or utilizing independent SONFH cohorts with well-matched tissues and comprehensive clinical data to validate key biomarkers; designing SZW intervention experiments to determine whether IKBKB and PRKCA serve as response targets of the formula in cellular or animal models; elucidating the specific roles of these two genes in SONFH pathogenesis and progression through gain- and loss-of-function experiments at the mechanistic level; and conducting rigorous external validation of the nomogram model, including comparative evaluations against conventional clinical diagnostic methods, to facilitate its clinical implementation. These follow-up studies are expected to advance the current correlation-based findings into causal mechanistic insights, thereby providing a stronger scientific foundation for the precise diagnosis and targeted therapy of SONFH.

5 Conclusion

This study leveraged public databases to download SONFH-related transcriptomic data, identifying 1,671 DEGs between the SONFH and control groups. Through network pharmacology, 69 therapeutic targets of SZW for SONFH were identified. The intersection of these 69 targets with the DEGs yielded 11 candidate genes. Machine learning, ROC curve analysis, and expression level validation were subsequently applied to identify two biomarkers (IKBKB and PRKCA) that indicate SZW's therapeutic effects on SONFH. Finally, the potential molecular mechanisms of these biomarkers as therapeutic targets for SONFH were explored through nomogram construction, GSEA enrichment analysis, immune infiltration analysis, molecular regulatory network analysis, and molecular docking. These findings provide a new theoretical framework for understanding the mechanism of SZW in treating SONFH. However, the effectiveness of these biomarkers in diagnosing and predicting SONFH requires further validation through large-sample clinical trials. Moreover, the regulatory roles of these biomarkers in SONFH need to be experimentally validated *in vivo*.

Data availability statement

The data presented in this study have been deposited in the Gene Expression Omnibus (GEO) database, with the accession numbers GSE123568 (available at <https://www.ncbi.nlm.nih.gov/geo/query/acc.cgi?acc=GSE123568>) and GSE74089 (available at <https://www.ncbi.nlm.nih.gov/geo/query/acc.cgi?acc=GSE74089>).

Ethics statement

The studies involving humans were approved by the Ethics Committee of Gansu University of Traditional Chinese Medicine Affiliated Hospital/Affiliated Hospital of Gansu University of Chinese Medicine. The studies were conducted in accordance with the local legislation and institutional requirements. The participants provided their written informed consent to participate in this study. Written informed consent was obtained from the individual(s) for the

publication of any potentially identifiable images or data included in this article.

Author contributions

TM: Conceptualization, Validation, Writing – original draft. DW: Funding acquisition, Methodology, Writing – review & editing. QX: Validation, Writing – review & editing. YL: Software, Writing – review & editing. JWa: Validation, Visualization, Writing – review & editing. XZ: Funding acquisition, Supervision, Writing – review & editing. LY: Formal analysis, Writing – review & editing. HH: Investigation, Writing – review & editing. XH: Resources, Writing – review & editing. XL: Data curation, Writing – review & editing. JL: Supervision, Writing – review & editing. HY: Conceptualization, Project administration, Writing – review & editing. JWu: Validation, Visualization, Writing – review & editing.

Funding

The author(s) declared that financial support was received for this work and/or its publication. This research was funded by the Gansu health industry Foundation (GSWSQNPY2024-16), the National Traditional Chinese Medicine Bone Injury Advantage Specialty Foundation of China (2023GS-05), the Gansu Provincial Natural Science Foundation (24JRRA554 and 24JRRA1036), and the Lanzhou Science and Technology Development Guidance Foundation (2023-2D-202).

Acknowledgments

We would like to express our sincere gratitude to all individuals and organizations who supported and assisted us throughout this research. Special thanks to the following authors: DW, JW, and HY. We would also like to express our gratitude to the Gansu Provincial Health Commission, the Gansu Provincial Department of Science and Technology, and the Lanzhou Municipal Department of Science and Technology for their support and funding of this article. In conclusion, we extend our thanks to everyone who has supported and assisted us along the way. Without your support, this research would not have been possible.

Conflict of interest

The author(s) declared that this work was conducted in the absence of any commercial or financial relationships that could be construed as a potential conflict of interest.

Generative AI statement

The author(s) declared that Generative AI was not used in the creation of this manuscript.

Any alternative text (alt text) provided alongside figures in this article has been generated by Frontiers with the support of artificial

intelligence and reasonable efforts have been made to ensure accuracy, including review by the authors wherever possible. If you identify any issues, please contact us.

Publisher's note

All claims expressed in this article are solely those of the authors and do not necessarily represent those of their affiliated organizations, or those of the publisher, the editors and the

reviewers. Any product that may be evaluated in this article, or claim that may be made by its manufacturer, is not guaranteed or endorsed by the publisher.

Supplementary material

The Supplementary material for this article can be found online at: <https://www.frontiersin.org/articles/10.3389/fmed.2026.1732825/full#supplementary-material>

References

- Zhao J, Zhang X, Guan J, Su Y, Jiang J. Identification of key biomarkers in steroid-induced osteonecrosis of the femoral head and their correlation with immune infiltration by bioinformatics analysis. *BMC Musculoskelet Disord.* (2022) 23:23. doi: 10.1186/s12891-022-04994-7
- Xu H, Fang L, Zeng Q, Chen J, Ling H, Xia H, et al. Glycyrrhizic acid alters the hyperoxidative stress-induced differentiation commitment of MSCs by activating the Wnt/B-catenin pathway to prevent SONFH. *Food Funct.* (2023) 14:946–60. doi: 10.1039/d2fo02337g
- Yang F, Zhang X, Song T, Li X, Lv H, Li T, et al. Huogu injection alleviates SONFH by regulating adipogenic differentiation of BMSCs via targeting the Mir-34c-5p/Mdm4 pathway. *Gene.* (2022) 838:146705. doi: 10.1016/j.gene.2022.146705
- Li L, Zhao S, Leng Z, Chen S, Shi Y, Shi L, et al. Pathological mechanisms and related markers of steroid-induced osteonecrosis of the femoral head. *Ann Med.* (2024) 56:56. doi: 10.1080/07853890.2024.2416070
- Çağlar S, Fatih Daşcı M, Acar A, Çağlar A, Mahsut Dinçel Y, Çataltepe A. Comparison of the prophylactic use of ibandronate and its use in early-stage osteonecrosis in rats with steroid-induced osteonecrosis of the femoral head. *Jt Dis Relat Surg.* (2023) 34:640–50. doi: 10.52312/jdrs.2023.1096
- Liu M, Ye J, Wu R, Luo D, Huang T, Dai D, et al. Shengxue busui decoction activates the Pi3k/Akt and Vegf pathways, enhancing vascular function and inhibiting osteocyte apoptosis to combat steroid-induced femoral head necrosis. *Front Pharmacol.* (2025) 15:1506594. doi: 10.3389/fphar.2024.1506594
- Jiang C, Zhou Z, Lin Y, Shan H, Xia W, Yin F, et al. Astragaloside IV ameliorates steroid-induced osteonecrosis of the femoral head by repolarizing the phenotype of pro-inflammatory macrophages. *Int Immunopharmacol.* (2021) 93:107345. doi: 10.1016/j.intimp.2020.107345
- Sun K, Xue Y, Zhang X, Li X, Zhao J, Xu X, et al. Tanshinone I alleviates steroid-induced osteonecrosis of femoral heads and promotes angiogenesis: in vivo and in vitro studies. *J Orthop Surg Res.* (2023) 18:474. doi: 10.1186/s13018-023-03934-y
- Ji W, Gong G, Liu Y, Liu Y, Zhang J, Li Q. Icarin promotes osteogenic differentiation of bone marrow mesenchymal stem cells (Bmscs) by activating Pi3k-Akt-Utx/Ezh2 signaling in steroid-induced femoral head osteonecrosis. *J Orthop Surg Res.* (2025) 20:20. doi: 10.1186/s13018-025-05697-0
- Yue J, Yu H, Liu P, Wen P, Zhang H, Guo W, et al. Preliminary study of icaritin indicating prevention of steroid-induced osteonecrosis of femoral head by regulating abnormal expression of Mirna-335 and protecting the functions of bone microvascular endothelial cells in rats. *Gene.* (2021) 766:145128. doi: 10.1016/j.gene.2020.145128
- Shan H, Lin Y, Yin F, Pan C, Hou J, Wu T, et al. Effects of Astragaloside iv on glucocorticoid-induced avascular necrosis of the femoral head via regulating Akt-related pathways. *Cell Prolif.* (2023) 56:e13485. doi: 10.1111/cpr.13485
- Du X, Wang X, Cui K, Chen Y, Zhang C, Yao K, et al. Tanshinone I and astragaloside IV inhibit Mir-223/Jak2/Stat1 signalling pathway to alleviate lipopolysaccharide-induced damage in nucleus pulposus cells. *Dis Markers* (2021) 2021:1–12. doi: 10.1155/2021/6554480, PMID: 34676010.
- Ma C, Wang Z, Mo L, Wang X, Zhou G, Yi C, et al. Tanshinone I attenuates estrogen-deficiency bone loss via inhibiting Rankl-induced Mapk and Nf-Kb signaling pathways. *Int Immunopharmacol.* (2024) 127:111322. doi: 10.1016/j.intimp.2023.111322
- Li Z-X, Zhuo J-L, Yang N, Gao M-B, Qu Z-H, Han T. Effect of *Lycium barbarum* polysaccharide on osteoblast proliferation and differentiation in postmenopausal osteoporosis. *Int J Biol Macromol.* (2024) 271:132415. doi: 10.1016/j.jbiomac.2024.132415
- Zou J, Qiu Z-C, Yu Q-Q, Wu J-M, Wang Y-H, Shi K-D, et al. Discovery of a potent antiosteoporotic drug molecular scaffold derived from *Angelica Sinensis* and its bioinspired Total synthesis. *ACS Cent Sci.* (2024) 10:628–36. doi: 10.1021/acscentsci.3c01414
- Zhu K, Liu W, Peng Y, Wang X, Wang Z, Zheng J, et al. Study on the mechanism of Shuanghe decoction against steroid-induced osteonecrosis of the femoral head: insights from network pharmacology, metabolomics, and gut microbiota. *J Orthop Surg Res.* (2025) 20:20. doi: 10.1186/s13018-025-05619-0
- Zhang P, Xu H, Wang P, Dong R, Xia C, Shi Z, et al. Yougui pills exert Osteoprotective effects on rabbit steroid-related osteonecrosis of the femoral head by activating B-catenin. *Biomed Pharmacother.* (2019) 120:120. doi: 10.1016/j.biopha.2019.109520
- Otasek D, Morris JH, Bouças J, Pico AR, Demchak B. Cytoscape automation: empowering workflow-based network analysis. *Genome Biol.* (2019) 20:185. doi: 10.1186/s13059-019-1758-4
- Chen H, Boutros PC. VennDiagram: a package for the generation of highly-customizable Venn and Euler diagrams in R. *BMC Bioinformatics.* (2011) 12:12. doi: 10.1186/1471-2105-12-35
- Ritchie ME, Phipson B, Wu D, Hu Y, Law CW, Shi W, et al. Limma powers differential expression analyses for Rna-sequencing and microarray studies. *Nucleic Acids Res.* (2015) 43:e47. doi: 10.1093/nar/gkv007
- Gustavsson EK, Zhang D, Reynolds RH, Garcia-Ruiz S, Ryten M, Mathelier A. Gtscript: an R package for the visualization and interpretation of transcript isoforms using ggplot2. *Bioinformatics.* (2022) 38:3844–6. doi: 10.1093/bioinformatics/btac409
- Gu ZER, Schlesner M. Complex Heatmaps reveal patterns and correlations in multidimensional genomic data. *Bioinformatics.* (2016) 32:2847–9. doi: 10.1093/bioinformatics/btw313
- Yu G, Wang L-G, Han Y, He Q-Y. Clusterprofiler: an R package for comparing biological themes among gene clusters. *OMICS.* (2012) 16:284–7. doi: 10.1089/omi.2011.0118
- Kang J, Choi YJ, Kim I-k, Lee HS, Kim H, Baik SH, et al. Lasso-based machine learning algorithm for prediction of lymph node metastasis in T1 colorectal cancer. *Cancer Res Treat.* (2021) 53:773–83. doi: 10.4143/crt.2020.974
- Hou N, Li M, He L, Xie B, Wang L, Zhang R, et al. Predicting 30-days mortality for mimic-iii patients with Sepsis-3: a machine learning approach using Xgboost. *J Transl Med.* (2020) 18:462. doi: 10.1186/s12967-020-02620-5
- Liu Y, Zhao Y, Zhang S, Rong S, He S, Hua L, et al. Developing a prognosis and chemotherapy evaluating model for Colon adenocarcinoma based on mitotic catastrophe-related genes. *Sci Rep.* (2024) 14:14. doi: 10.1038/s41598-024-51918-7
- Xu J, Yang T, Wu F, Chen T, Wang A, Hou S. A nomogram for predicting prognosis of patients with cervical Cerclage. *Heliyon.* (2023) 9:9. doi: 10.1016/j.heliyon.2023.e21147
- Wang P, Chen Q, Tang Z, Wang L, Gong B, Li M, et al. Uncovering Ferroptosis in Parkinson's disease via bioinformatics and machine learning, and reversed deducing potential therapeutic natural products. *Front Genet.* (2023) 14:14. doi: 10.3389/fgene.2023.1231707
- Zhou J, Huang J, Li Z, Song Q, Yang Z, Wang L, et al. Identification of aging-related biomarkers and immune infiltration characteristics in osteoarthritis based on bioinformatics analysis and machine learning. *Front Immunol.* (2023) 14:14. doi: 10.3389/fimmu.2023.1168780
- Wang L, Wang D, Yang L, Zeng X, Zhang Q, Liu G, et al. Cuproptosis related genes associated with Jab1 shapes tumor microenvironment and pharmacological profile in nasopharyngeal carcinoma. *Front Immunol.* (2022) 13:13. doi: 10.3389/fimmu.2022.989286
- Zhai Z, Tao X, Alami MM, Shu S, Wang X. Network pharmacology and molecular docking combined to analyze the molecular and pharmacological mechanism of *Pinellia Ternata* in the treatment of hypertension. *Curr Issues Mol Biol.* (2021) 43:65–78. doi: 10.3390/cimb43010006
- Chang J, Wu H, Wu J, Liu M, Zhang W, Hu Y, et al. Constructing a novel mitochondrial-related gene signature for evaluating the tumor immune microenvironment and predicting survival in stomach adenocarcinoma. *J Transl Med.* (2023) 21:21. doi: 10.1186/s12967-023-04033-6
- Jiang W, Chen Y, Sun M, Huang X, Zhang H, Fu Z, et al. Lncrna Dgcr5-encoded polypeptide rip aggravates Sonfh by repressing nuclear localization of B-catenin in Bmsc. *Cell Rep.* (2023) 42:42. doi: 10.1016/j.celrep.2023.112969
- Sacco K, Kuehn HS, Kawai T, Alsaati N, Smith L, Davila B, et al. A heterozygous gain-of-function variant in Ikbkb associated with autoimmunity and autoinflammation. *J Clin Immunol.* (2022) 43:512–20. doi: 10.1007/s10875-022-01395-2

35. Luo D, Gao X, Zhu X, Wu J, Yang Q, Xu Y, et al. Identification of steroid-induced osteonecrosis of the femoral head biomarkers based on immunization and animal experiments. *BMC Musculoskelet Disord.* (2024) 25:596. doi: 10.1186/s12891-024-07707-4
36. Li ZW, Omori SA, Labuda T, Karin M, Rickert RC. Ikk beta is required for peripheral B cell survival and proliferation. *J Immunol.* (2003) 170:4630–7. doi: 10.4049/jimmunol.170.9.4630
37. Bhattacharyya S, Sen P, Wallet M, Long B, Baldwin AS Jr, Tisch R. Immunoregulation of dendritic cells by Il-10 is mediated through suppression of the Pi3k/Akt pathway and of Ikappab kinase activity. *Blood.* (2004) 104:1100–9. doi: 10.1182/blood-2003-12-4302
38. Timmer AM, Nizet V. Ikkbeta/Nf-Kappab and the miscreant macrophage. *J Exp Med.* (2008) 205:1255–9. doi: 10.1084/jem.20081056
39. Liu Y, Shan H, Zong Y, Lin Y, Xia W, Wang N, et al. Ikke in osteoclast inhibits the progression of methylprednisolone-induced osteonecrosis. *Int J Biol Sci.* (2021) 17:1353–60. doi: 10.7150/ijbs.57962
40. Xu Y, Zhang S, Liao X, Li M, Chen S, Li X, et al. Circular Rna Circikkb promotes breast Cancer bone metastasis through sustaining Nf-Kb/bone remodeling factors signaling. *Mol Cancer.* (2021) 20:98. doi: 10.1186/s12943-021-01394-8
41. Cardinez C, Miraghadzadeh B, Tanita K, da Silva E, Hoshino A, Okada S, et al. Gain-of-function Ikkbb mutation causes human combined immune deficiency. *J Exp Med.* (2018) 215:2715–24. doi: 10.1084/jem.20180639
42. Kim A, Nam YJ, Lee CS. Taxifolin reduces the cholesterol oxidation product-induced neuronal apoptosis by suppressing the Akt and Nf-Kb activation-mediated cell death. *Brain Res Bull.* (2017) 134:63–71. doi: 10.1016/j.brainresbull.2017.07.008
43. Lu QY, Guo L, Zhang QY, Yang FM, Zhou ST, Sun QY. Luteolin alleviates the Tnf- α -induced inflammatory response of human microvascular endothelial cells via the Akt/Mapk/Nf-Kb pathway. *Mediat Inflamm.* (2024) 2024:6393872. doi: 10.1155/mi/6393872
44. Zhu QJWJ, Li Y, Bai ZJ, Guo XB, Pan T. Prkca promotes mitophagy through the Mir-15a-5p/Pdk4 axis to relieve sepsis-induced acute lung injury. *Infect Immun.* (2023) 91:e0046522. doi: 10.1128/iai.00465-22
45. Sun T, Zhang P, Zhang Q, Wang B, Zhao Q, Liu F, et al. Transcriptome analysis reveals Prkca as a potential therapeutic target for overcoming cisplatin resistance in lung cancer through ferroptosis. *Heliyon.* (2024) 10:e30780. doi: 10.1016/j.heliyon.2024.e30780
46. Nakura A, Higuchi C, Yoshida K, Yoshikawa H. Pkca suppresses osteoblastic differentiation. *Bone.* (2011) 48:476–84. doi: 10.1016/j.bone.2010.09.238
47. Kim HH, Kim JH, Kwak HB, Huang H, Han SH, Ha H, et al. Inhibition of osteoclast differentiation and bone resorption by Tanshinone Iia isolated from *Salvia Miltiorrhiza* Bunge. *Biochem Pharmacol.* (2004) 67:1647–56. doi: 10.1016/j.bcp.2003.12.031
48. Zhang Z, Kumar V, Dybkov O, Will CL, Zhong J, Ludwig SEJ, et al. Structural insights into the cross-exon to cross-intron spliceosome switch. *Nature.* (2024) 630:1012–9. doi: 10.1038/s41586-024-07458-1
49. Long F, Li L, Xie C, Ma M, Wu Z, Lu Z, et al. Intergenic Circrna Circ_0007379 inhibits colorectal Cancer progression by modulating Mir-320a biogenesis in a Ksrp-dependent manner. *Int J Biol Sci.* (2023) 19:3781–803. doi: 10.7150/ijbs.85063
50. Gu C, Wang W, Tang X, Xu T, Zhang Y, Guo M, et al. Chek1 and Circchek1_246aa evoke chromosomal instability and induce bone lesion formation in multiple myeloma. *Mol Cancer.* (2021) 20:20. doi: 10.1186/s12943-021-01380-0
51. Mao G, Xu Y, Long D, Sun H, Li H, Xin R, et al. Exosome-transported Circrna_0001236 enhances Chondrogenesis and suppress cartilage degradation via the Mir-3677-3p/Sox9 Axis. *Stem Cell Res Ther.* (2021) 12:12. doi: 10.1186/s13287-021-02431-5
52. Yang Y, Yujiao W, Fang W, Linhui Y, Ziqi G, Zhichen W, et al. The roles of Mirna, Lncrna and Circrna in the development of osteoporosis. *Biol Res.* (2020) 53:40. doi: 10.1186/s40659-020-00309-z
53. Chen K, Liu Y, He J, Pavlos N, Wang C, Kenny J, et al. Steroid-induced osteonecrosis of the femoral head reveals enhanced reactive oxygen species and hyperactive osteoclasts. *Int J Biol Sci.* (2020) 16:1888–900. doi: 10.7150/ijbs.40917
54. Krishnacoumar B, Stenzel M, Garibagaoglu H, Omata Y, Sworn RL, Hofmann T, et al. Caspase-8 promotes scramblase-mediated phosphatidylserine exposure and fusion of osteoclast precursors. *Bone Res.* (2024) 12:40. doi: 10.1038/s41413-024-00338-4
55. Zhang QAI, Liu S, Chen C, Shi S, Shi S, Le AD. Il-17-mediated M1/M2 macrophage alteration contributes to pathogenesis of bisphosphonate-related osteonecrosis of the jaws. *Clin Cancer Res.* (2013) 19:3176–88. doi: 10.1158/1078-0432.CCR-13-0042
56. Ma JGJ, Gao F, Wang B, Yue D, Sun W, Wang W. The role of immune regulatory cells in nontraumatic osteonecrosis of the femoral head: a retrospective clinical study. *Biomed Res Int.* (2019) 2019:1302015. doi: 10.1155/2019/1302015
57. Cao YJC, Wang X, Wang H, Yan Z, Yuan H. Reciprocal effect of Microrna-224 on osteogenesis and adipogenesis in steroid-induced osteonecrosis of the femoral head. *Bone.* (2021) 145:115844. doi: 10.1016/j.bone.2021.115844
58. Kong L, Zuo R, Wang M, Wang W, Xu J, Chai Y, et al. Silencing Microrna-137-3p, which targets Runx2 and Cxcl12 prevents steroid-induced osteonecrosis of the femoral head by facilitating osteogenesis and angiogenesis. *Int J Biol Sci.* (2020) 16:655–70. doi: 10.7150/ijbs.38713
59. Zhang F, Peng W, Wang T, Zhang J, Dong W, Wang C, et al. Lnc Tmem235 promotes repair of early steroid-induced osteonecrosis of the femoral head by inhibiting hypoxia-induced apoptosis of Bmscs. *Exp Mol Med.* (2022) 54:1991–2006. doi: 10.1038/s12276-022-00875-0
60. Zhang XLH, Kourkoumelis N, Wu Z, Li G, Shang X. Comprehensive analysis of Lncrna and Mirna expression profiles and Cerna network construction in osteoporosis. *Calcif Tissue Int.* (2020) 106:343–54. doi: 10.1007/s00223-019-00643-9

Glossary

SONFH - Steroid-induced osteonecrosis of the femoral head	ROC - Receiver operating characteristic
SZW - Shenggu Zaizao Wan	FDR - False discovery rate
DEGs - Differentially expressed genes	IKBKB - Inhibitor of nuclear factor kappa b kinase subunit beta
GSEA - Gene set enrichment analysis	PRKCA - Protein kinase C alpha
RT-qPCR - Real-time quantitative reverse transcription PCR	NIK - Nf-kb-inducing kinase
TCM - Traditional Chinese medicine	LPS - Lipopolysaccharide
GEO - Gene expression omnibus	circRNAs - Circular RNAs
TCMSP - Traditional Chinese medicine systems pharmacology database	miRNAs - MicroRNAs
HERB - Herbal encyclopedia for research on bioactivity	RBPs - RNA-binding proteins
TsI - Tanshinone I	OB - Oral bioavailability
KEGG - Kyoto encyclopedia of genes and genomes	DL - Drug likeness
PPI - Protein-protein interaction	FC - Foldchange
GO - Gene ontology	STRING - Search tool for the retrieval of interacting genes and proteins
BPs - Biological processes	HL - Hosmer-Lemeshow
CCs - Cellular components	AUC - Area under curve
MFs - Molecular functions	DICs - Differential immune cells
LASSO - Least absolute shrinkage and selection operator	TFs - Transcription factors
SVM-RFE - Support vector machine recursive feature elimination	cDNA - Complementary DNA